Bioconjugate Chemistry

Article

pubs.acs.org/bc

Anti-CEA Antibody Fragments Labeled with [^{18}F]AlF for PET Imaging of CEA-Expressing Tumors

S. Lütje,[†,*] G. M. Franssen,[†] R. M. Sharkey,[‡] P. Laverman,[†] E. A. Rossi,[‡] D. M. Goldenberg,[‡] W. J. G. Oyen,[†] O. C. Boerman,[†] and W. J. McBride[‡]

[†]Department of Nuclear Medicine, Radboud University Medical Center, Nijmegen, The Netherlands

[‡]Immunomedics, Inc., Morris Plains, New Jersey 07950, United States

ABSTRACT: A facile and rapid method to label peptides with ^{18}F based on chelation of [^{18}F]AlF has been developed recently. Since this method requires heating to 100 °C, it cannot be used to label heat-sensitive proteins. Here, we used a two-step procedure to prepare ^{18}F-labeled heat-labile proteins using the [^{18}F]AlF method based on hot maleimide conjugation. 1,4,7-Triazacyclononae-1,4-diacetate (NODA) containing a methyl phenylacetic acid group (MPA) functionalized with *N*-(2-aminoethyl)maleimide (EM) was used as a ligand which was labeled with [^{18}F]AlF and then conjugated to the humanized anti-CEA antibody derivatives hMN-14-Fab′, hMN-14-(scFv)$_2$ (diabody), and a Dock-and-Lock engineered dimeric fragment hMN-14 Fab-AD2 at room temperature. The *in vivo* tumor targeting characteristics of the ^{18}F-labeled antibody derivatives were determined by PET imaging of mice with s.c. xenografts. NODA-MPAEM was radiolabeled with [^{18}F]AlF at a specific activity of 29−39 MBq/nmol and a labeling efficiency of 94 ± 2%. The labeling efficiencies of the maleimide conjugation ranged from 70% to 77%, resulting in [^{18}F]AlF-labeled hMN14-Fab′, hMN14-Fab-AD2, or hMN14-diabody with a specific activity of 15−17 MBq/nmol. The radiolabeled conjugates were purified by gel filtration. For biodistribution and microPET imaging, antibody fragments were injected intravenously into BALB/c nude mice with s.c. CEA-expressing LS174T xenografts (right flank) and CEA-negative SK-RC-52 xenografts (left flank). All [^{18}F]AlF-labeled conjugates showed specific uptake in the LS174T xenografts with a maximal tumor uptake of 4.73% ID/g at 4 h after injection. Uptake in CEA-negative SK-RC-52 xenografts was significantly lower. Tumors were clearly visualized on microPET images. Using a [^{18}F]AlF-labeled maleimide functionalized chelator, antibody fragments could be radiofluorinated within 4 h at high specific activity. Here, we translated this method to preclinical PET imaging studies and showed feasibility of [^{18}F]AlF-fluorinated hMN-14-Fab′, [^{18}F]AlF-hMN-14-Fab-AD2, and [^{18}F]AlF-hMN-14-diabody for microPET imaging of CEA-expressing colonic cancer.

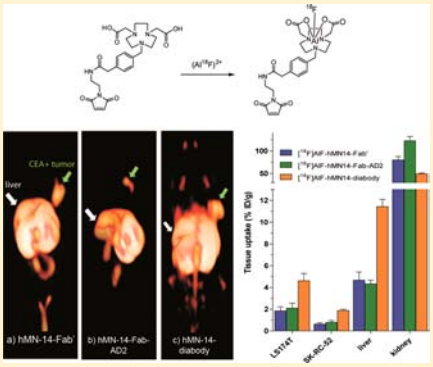

INTRODUCTION

Positron emission tomography (PET) has evolved as a prominent molecular imaging modality in oncology, since it allows high sensitivity and quantitative imaging of cellular features and processes.[1] ^{18}F is an ideal radionuclide for PET imaging, because of its low positron energy, the lack of other emissions, and its half-life of 109.8 min. The most commonly used tracer for PET imaging of tumors is 2-[^{18}F]fluoro-2-deoxyglucose ([^{18}F]FDG), which exploits the increased glucose metabolism of tumor cells.

Previously, ^{18}F-radiolabeling of peptides was a time-consuming and inefficient multistep process. By exploiting the strong bond between [^{18}F]-fluoride and Al^{3+}, ^{18}F-radiolabeling can be performed efficiently in one step by chelating [^{18}F]AlF.[2] This method could only be applied to peptides and heat-stable proteins, because 100 °C is the optimal labeling temperature. By separating the chelation of [^{18}F]AlF (at 100 °C) from the conjugation to the targeting molecule (at room temperature), the labeling approach can now also be applied to label heat-sensitive proteins with ^{18}F.[3] In this approach, the [^{18}F]AlF-chelating moiety 1,4,7-triazacyclonona-1,4-diacetate (NODA) with a methyl phenylacetic acid group (MPA) functionalized with *N*-(2-aminoethyl)maleimide (EM) is used. NODA-MPAEM can be labeled efficiently with ^{18}F (at 100−110 °C) and subsequently be conjugated with the heat-sensitive protein at room temperature via a maleimide−thiol reaction.

Although intact antibodies are not suitable for imaging of cancer with ^{18}F because their accumulation in tumors generally takes several days, smaller antibody fragments such as Fab′, F(ab′)$_2$, and scFv, allow imaging of tumor lesions within several hours after injection, which is compatible with the half-life of ^{18}F. Since Fab′ fragments bind monovalently to target regions, which might have a negative impact on the tumor uptake and retention, we included the divalent (scFv)$_2$ diabody format of hMN-14 in our studies, which may provide more avid binding to the target.

In this study, we applied the 2-step method to prepare [^{18}F]-AlF-fluorinated NODA-MPAEM-hMN-14-Fab′, NODA-

Received: October 25, 2013
Revised: December 30, 2013
Published: January 1, 2014

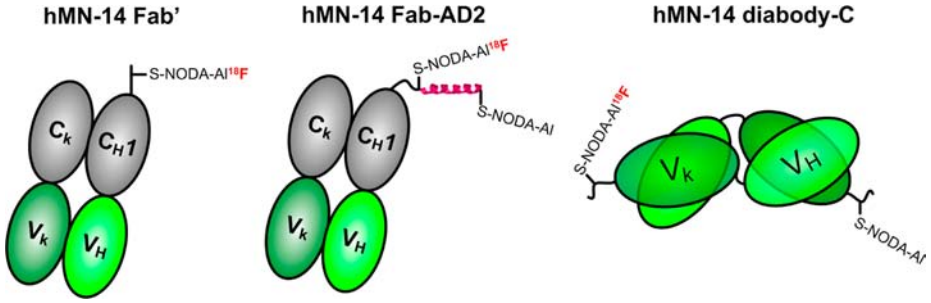

Figure 1. Schematic representation of hMN-14 Fab′, hMN-14 Fab-AD2, and hMN-14-diabody. To represent incomplete ^{18}F-labeling due to a limited amount of ^{18}F that was used, ^{18}F was added to only half of the Al moieties in this schematic drawing.

MPAEM-hMN-14-Fab-AD2, and NODA-MPAEM-hMN-14-diabody and evaluated the *in vitro* characteristics and the *in vivo* tumor targeting capacities of these tracers in nude mice with CEA-expressing LS174T human colon carcinoma xenografts.

MATERIALS AND METHODS

Antibody Derivatives. The monoclonal antibody hMN-14 (labetuzumab) and hMN-14-Fab′, hMN-14-Fab-AD2, and hMN-14-diabody (Figure 1) were obtained from Immunomedics, Inc. (Morris Plains, NJ, USA).

Synthesis of NODA-MPAEM. NODA-MPEAM (methyl phenyl acetamido ethyl maleimide, Figure 2) was synthesized as

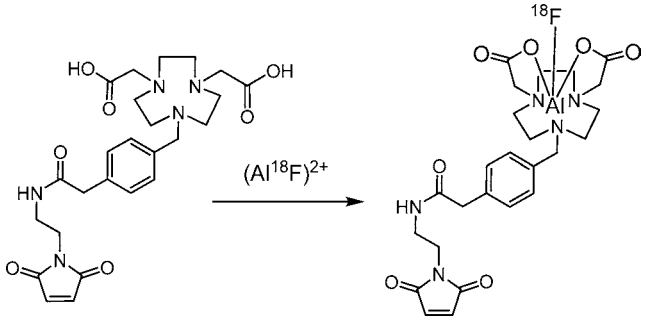

Figure 2. Labeling of NODA-MPAEM with ^{18}F. The nitrogen atom coordination with Al is not illustrated in this figure.

described by McBride et al.[2] Briefly, $(t\text{Bu})_2$NODA-MPAA NHS ester (128.3 mg, 0.213 mmol) in CH_2Cl_2 (5 mL) was added to a solution of *N*-(2-aminoethyl) maleimide trifluoroacetate salt (52.6 mg, 0.207 mmol) in 250 μL of dimethylformamide (DMF) and 20 μL of *N*,*N*-diisopropylethylamine (DIEA). After 3 h of incubation, the conjugation was evaporated and treated with 2 mL of trifluoroacetic acid (TFA). In the following, the product was diluted with water and purified by preparative RP-HPLC using a Waters PrepLC 4000 system with a Sunfire Prep C18 optimal bed density (OBD) reverse-phase column (150 mm × 30 mm, 5 μm),using a linear gradient of 100% A (0.1% TFA) to 15% B (90% acetonitrile, 10% water, 0.1% TFA) over 80 min at a flow rate of 45 mL/min (absorbance 220 nm).

^{18}F Radiolabeling of NODA-MPAEM. ^{18}F dissolved in water (BV Cyclotron VU, Amsterdam, The Netherlands) was passed through a SepPak CM cartridge (Waters, Etten-Leur, The Netherlands) and a Sep-Pak QMA cartridge (Waters, Etten-Leur, The Netherlands), that were both preconditioned with 10 mL of metal-free water. After removing the CM cartridge, ^{18}F was eluted from the QMA cartridge with 0.9% NaCl. Subsequently, 75 μL of eluate (1.94−2.05 GBq) was mixed with $AlCl_3$ (40 nmol in 30 μL of 2 mM NaAc (pH 4.2)) and dissolved in 1.0 M NaAc (pH 4.2). After 10 min of incubation at room temperature, acetonitrile (300 μL) and NODA-MPAEM ligand (40 nmol), dissolved in 2 mM NaAc (pH 4.2), were added and incubated for 20 min at 106 °C. After incubation, the labeling mixture was evaporated to dryness and 100 μL of PBS was added. Labeling efficiency was determined by RP-HPLC (Agilent 1200 Series, Amstelveen, Netherlands) on a C18 Onyx monolithic column (4.6 mm × 100 mm, Phenomenex, Torrance, USA) in a gradient from H_2O/0.1% TFA to acetronitrile/0.1%TFA.

Conjugation of [^{18}F]AlF-NODA-MPAEM to anti-CEA Antibody Fragments. [^{18}F]AlF-NODA-MPAEM (22−23 nmol, 538−625 MBq) was conjugated to humanized anti-CEA antibody fragments, hMN-14 Fab′ (20 nmol), hMN-14-Fab-AD2 (20 nmol), and hMN-14-diabody (20 nmol) in 100 μL of PBS, 2 mM EDTA. After incubating for 20 min at room temperature, labeling efficiency was determined by instant thin-layer chromatography, with 0.1 mol/L citrate buffer (pH 6.0), as the mobile phase. The reaction mixture was purified on a PD-10 column (GE Healthcare, Little Chalfont, United Kingdom) eluted with PBS, 0.5% bovine serum albumin (BSA). In all experiments, the labeling efficiency of the ^{18}F-labeled antibody preparations was determined by instant thin layer chromatography and exceeded 95%. The radiochemical purity of the [^{18}F]AlF fluorinated antibody fragments was determined by FPLC analysis using an ÄKTApurifier UPC-10 FPLC system (GE Healthcare Life Sciences, Little Chalfont, U.K.) with a BioSEP SEC s3000 column (300 mm × 7.8 mm, Phenomonex, Torrance, California, USA) using PBS as eluent at a flow rate of 1 mL/min. For all [^{18}F]AlF fluorinated antibody fragments, single peaks have been observed on FPLC analysis.

Cell Culture. The human colorectal carcinoma cell line LS174T (CEA-positive) and the renal cell carcinoma cell line, SK-RC-52 (CEA-negative), were used. Both cell lines were cultured in RPMI 1640 medium, supplemented with 10% fetal calf serum (Life Technologies, Bleiswijk, The Netherlands).

Immunoreactivity and IC_{50}. The immunoreactive fractions of the ^{18}F-labeled antibody preparations were determined using freshly trypsinized LS174T cells, as described by Lindmo et al.[4] with minor modifications: after 1 h of incubation at 37 °C, the activity in the vials and after washing with 500 μL of binding buffer in the cell pellet was determined in the γ-counter (Wizard^2 Automatic Gamma Counter, PerkinElmer, Waltham, MA). The IC_{50} of hMN-14 IgG, hMN-14-Fab′, hMN-14-Fab-AD2, and hMN-14-diabody was determined in a competitive binding assay on LS174T cells that were grown to confluency in six-well plates. Cells were incubated on ice for 2.5 h in 1 mL

dx.doi.org/10.1021/bc4004926 | *Bioconjugate Chem.* 2014, 25, 335−341

of binding buffer with 1 kBq of the ^{111}In-labeled hMN-14 IgG. A concentration range from 0.1 to 300 nM of hMN-14 IgG, hMN-14-Fab′, hMN-14-Fab-AD2, or hMN-14-diabody was added immediately before addition of ^{111}In-labeled hMN-14 IgG. After incubation, cells were washed with binding buffer, and cell-associated activity was measured in a γ-counter. IC_{50} values were calculated using GraphPad Prism software, version 5.03 (GraphPad, La Jolla, USA).

Mouse Model. Female BALB/c nude mice (Janvier, Le Genest Saint Isle, France), 8−9 weeks old, were housed in IVC cages (5 mice per cage) under nonsterile standard conditions with free access to standard animal chow and water. After one week of adaption to laboratory conditions, mice were inoculated subcutaneously with 1×10^6 CEA-expressing LS174T cells (right flank) and with 3×10^6 CEA-negative SK-RC-52 cells (left flank), both suspended in 200 μL of complete RPMI 1640 medium. SK-RC-52 cells were inoculated 10 days prior to LS174T cells. Both tumors grew to approximately 0.1 g in 21 and 11 days after tumor cell inoculation, respectively. All experiments were approved by the institutional Animal Welfare Committee of the Radboud University, and were conducted in accordance to the principles set forth by the Revised Dutch Act on Animal Experimentation.

Biodistribution Studies. To evaluate the *in vivo* tumor targeting characteristics and perform microPET imaging of the [^{18}F]AlF-labeled antibody preparations, 1 nmol of [^{18}F]AlF-hMN-14-Fab′ (14 MBq/mouse, n = 5), [^{18}F]AlF-hMN-14-Fab-AD2 (17 MBq/mouse, n = 5), and [^{18}F]AlF-hMN-14-diabody (15 MBq/mouse, n = 4) were injected i.v. into mice bearing LS174T tumors and SK-RC-52 xenografts. One additional group of 4 mice received [^{18}F]FDG (15.0 MBq/mouse) intravenously.

In addition, for all antibody fragment preparations, separate groups of 3−5 mice received an excess of unlabeled hMN-14 IgG (3.2 nmol/mouse) three days before injection of the [^{18}F]AlF-labeled antibody preparation. Mice were euthanized by CO_2/O_2 asphyxiation, and the biodistribution of the antibody preparations was determined 4 h after injection. Blood samples were obtained by cardiac puncture, tissues were dissected and weighed, and the radioactivity was measured in a γ-counter. For calculation of the uptake of radioactivity in each tissue as a fraction of the injected dose, an aliquot of the injection dose was counted simultaneously.

microPET Imaging. The above-described groups of female BALB/c nude mice were imaged on an Inveon microPET/CT scanner (Siemens Preclinical Solutions, Knoxville, TN) at 4 h after injection. MicroPET images were acquired under general anesthesia (isoflurane/O_2) for 20 min. After the scanning procedure, mice were euthanized by CO_2/O_2 asphyxiation and the biodistribution of the radiolabel was determined. Activity concentrations in the tissues (percentage of the injected dose per gram; % ID/g) were determined as described above. The microPET scans were reconstructed with Inveon Acquisition Workplace software (version 1.5; Siemens Preclinical Solutions), using a 3-dimensional fast maximum a posteriori algorithm with the following parameters: matrix, 256 × 256 × 161; pixel size, 0.4 × 0.4 × 0.8 mm; and β-value of 1.5 mm resolution with uniform variance.

Statistical Analysis. Statistical analyses were performed with Graphpad Prism, version 5.03 (GraphPad, La Jolla, CA). Results are presented as mean ± standard deviation (SD). Differences in tumor uptake of the antibody preparations were tested for significance using the statistical tests, as indicated in the Results section. A p-value below 0.05 was considered significant.

RESULTS

Radiolabeling. The NODA-MPAEM ligand could be labeled rapidly (<60 min) and efficiently at a specific activity of 29−39 MBq/nmol with a labeling efficiency of 94 ± 2%. The efficiencies of the maleimide conjugation were 70% ([^{18}F]AlF-hMN-14-Fab′), 77% ([^{18}F]AlF-hMN-14-Fab-AD2), and 77% ([^{18}F]AlF-hMN-14-diabodies), respectively, resulting in [^{18}F]AlF-labeled hMN-14 antibody fragment derivatives with a specific activity of 15−17 MBq/nmol (Table 1). Radiochemical purity exceeded 95%.

Table 1. Summary of the Results of Radiolabeling of [^{18}F]ALF-NODA-MPAEM and Hot Conjugation with the hMN14 Antibody Fragments Fab′, Fab-AD2, and Diabody[a]

	[^{18}F]AlF-hMN14-Fab′	[^{18}F]AlF-hMN14-Fab-AD2	[^{18}F]AlF-hMN14-diabody
specific activity (MBq/nmol)	18	23	20
overall labeling efficiency (%)	66	71	71
yield after purification (%)	49	59	66
immunoreactive fraction	>60	>60	>60
IC_{50} value (nM)	11.2 ± 1.3	26.9 ± 1.3	7.9 ± 1.2

[a]The IC_{50} of hMN14-IgG was 8.3 ±1.5 nM and serves as a reference for the antibody fragments.

Immunoreactivity and IC_{50}. The immunoreactive fractions of [^{18}F]AlF-hMN-14-Fab′, [^{18}F]AlF-hMN-14-Fab-AD2, and [^{18}F]AlF-hMN-14-diabodies as determined *in vitro* exceeded 60%. The IC_{50} of hMN-14 IgG, which was included as a reference, was 8.3 ± 1.5 nM. The IC_{50} values of hMN-14-Fab′ (11.2 ± 1.3 nM) and hMN-14-diabody (7.9 ± 1.2 nM) were comparable to that of hMN-14 IgG, while the IC_{50} of hMN14-Fab-AD2 (IC_{50} 26.9 ± 1.3 nM) was slightly higher (Table 1).

microPET Imaging. 3D-rendered microPET images of all [^{18}F]AlF-labeled antibody formats in mice with tumors are displayed in Figure 3. At 4 h after injection specific uptake of the antibody formats was observed in the CEA$^+$ LS174T tumors (right flank). Tumors were imaged clearly with all three [^{18}F]AlF-fluorinated antibody formats. However, based on visual nonquantitative analysis, the clearest visualization of the CEA$^+$ tumors with specific contrast to background tissue has been obtained with the [^{18}F]AlF-hMN-14-Fab′ and [^{18}F]AlF-hMN-14-Fab-AD2 formats, which is in concordance with the observed higher tumor-to-blood ratios of these formats. In addition, for all three antibody formats, high kidney and liver uptake was observed.

The uptake in the CEA$^-$ SK-RC-52 xenografts (left flank) remained low for all antibody formats and could not be visualized with microPET imaging.

Biodistribution Studies. The results of the biodistribution studies with [^{18}F]AlF-hMN-14-Fab′, [^{18}F]AlF-hMN-14-Fab-AD2, and [^{18}F]AlF-hMN-14-diabodies in nude mice with s.c. CEA$^+$ LS174T xenografts (right flank) and CEA$^-$ SK-RC-52 xenografts (left flank) after dissection are summarized in Figure 4. The biodistribution of [^{18}F]FDG was determined in the same model as a reference. At 4 h after injection, all antibody

dx.doi.org/10.1021/bc4004926 | Bioconjugate Chem. 2014, 25, 335−341

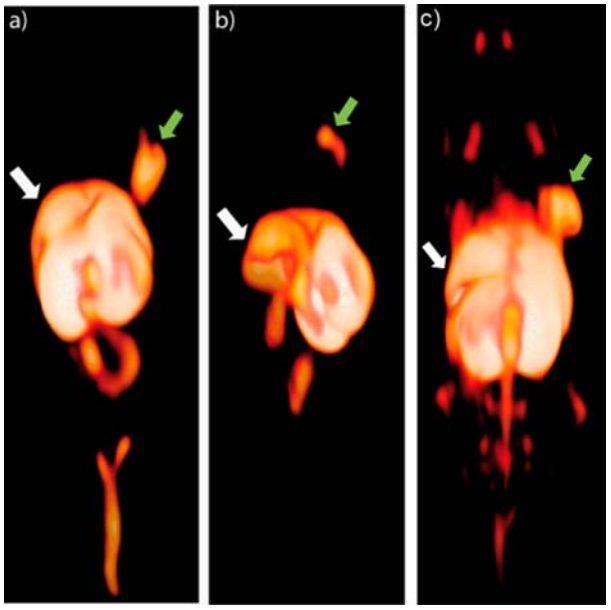

Figure 3. 3D-rendered microPET scans of (a) [^{18}F]AlF-NODA-MPAEM-hMN-14-Fab′, (b) [^{18}F]AlF-NODA-MPAEM-hMN-14-Fab-AD2, and (c) [^{18}F]AlF-NODA-MPAEM-hMN-14-diabody in mice with s.c. LS174T (right flank, green arrow) and SK-RC-52 (left flank) xenografts. The white arrows indicate the liver.

preparations showed preferential accumulation in the CEA$^+$ LS174T tumors, reaching 1.85 ± 0.36% ID/g, 2.10 ± 0.46% ID/g, and 4.61 ± 0.67% ID/g for [^{18}F]AlF-hMN-14-Fab′, [^{18}F]AlF-hMN-14-Fab-AD2, and [^{18}F]AlF-hMN-14-diabody (Figure 4). Uptake in the negative control tumors remained significantly lower for all antibody formats, indicating the specific targeting of the antibody formats to CEA-expressing tumor. For all fragments, tumor uptake could be blocked by injection of an excess of unlabeled hMN14 IgG, resulting in non-CEA-mediated uptake of 0.59 ± 0.12% ID/g, 0.68 ± 0.13% ID/g, and 1.37 ± 0.04% ID/g for [^{18}F]AlF-hMN-14-Fab′, [^{18}F]AlF-hMN-14-Fab-AD2, and [^{18}F]AlF-hMN-14-diabody, respectively, at 4 h after injection.

Tumor-to-blood ratios at 4 h after injection were significantly higher for [^{18}F]AlF-hMN-14-Fab′ and [^{18}F]AlF-hMN-14-Fab-AD2 compared to the [^{18}F]AlF-hMN-14-diabody format, reaching 5.87 ± 0.93 ($p < 0.005$), 6.15 ± 1.58 ($p = 0.01$), and 2.75 ± 0.18, respectively. Tumor-to-blood ratios of [^{18}F]FDG were 3.70 ± 0.38, which is significantly lower compared to those of [^{18}F]AlF-hMN-14-Fab′ ($p < 0.005$) and [^{18}F]AlF-hMN-14-Fab-AD2 ($p < 0.05$).

CEA$^+$-to-CEA$^-$ tumor uptake ratios (localization index) for [^{18}F]AlF-hMN-14-Fab′, [^{18}F]AlF-hMN-14-Fab-AD2, [^{18}F]AlF-hMN-14-diabody, and [^{18}F]FDG were 3.1 ± 0.9, 2.7 ± 0.7, 2.5 ± 0.3, and 2.1 ± 0.4, respectively (Figure 5). Tumor-to-muscle ratios obtained with the [^{18}F]AlF-hMN-14-diabody format, [^{18}F]AlF-hMN-14-Fab′ and [^{18}F]AlF-hMN-14-Fab-AD2, were comparable with 15.5 ± 2.3, 14.3 ± 3.9, and 14.0 ± 5.3, respectively.

All antibody preparations showed high kidney retention. Renal accumulation was highest for [^{18}F]AlF-hMN-14-Fab-AD2 (122.6 ± 9.4% ID/g), while kidney uptake of [^{18}F]AlF-hMN-14-Fab′ was lower (90.7 ± 7.0% ID/g) ($p < 0.005$). The lowest renal accumulation was observed for the [^{18}F]AlF-hMN-14-diabody format (57.4 ± 5.5% ID/g) ($p < 0.01$).

All [^{18}F]AlF-labeled antibody derivatives showed high hepatic uptake. The liver uptake of [^{18}F]AlF-hMN-14-Fab′ (4.36 ± 0.57% ID/g) and [^{18}F]AlF-hMN-14-Fab-AD2 (4.32 ± 0.35% ID/g) was significantly lower compared to the liver uptake of the [^{18}F]AlF-hMN-14-diabody format (11.1 ± 1.0% ID/g) ($p < 0.05$).

DISCUSSION

In this study, we applied a two-step method to prepare [^{18}F]-AlF-fluorinated NODA-MPAEM-hMN-14-Fab′, NODA-MPAEM-hMN-14-Fab-AD2, and NODA-MPAEM-hMN-14-diabody, and we evaluated the *in vitro* characteristics and the *in vivo* tumor targeting capacities of these tracers in nude mice with CEA-expressing LS174T human colon carcinoma

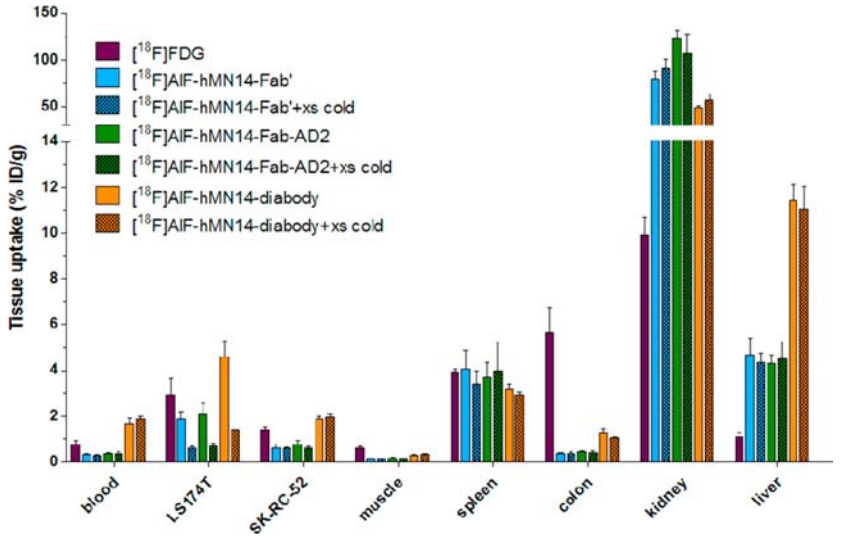

Figure 4. Biodistribution of [^{18}F]-FDG, [^{18}F]AlF-hMN-14-Fab′, [^{18}F]AlF-hMN-14-Fab-AD2, and [^{18}F]AlF-hMN-14-diabody in several tissues and subcutaneous LS174T and SK-RC-52 tumor xenografts in mice. For [^{18}F]AlF-hMN-14-Fab′, [^{18}F]AlF-hMN-14-Fab-AD2, and [^{18}F]AlF-hMN-14-diabody, an excess of unlabeled hMN-14 IgG (500 μg/mouse, xs) was injected 3 days before injection of the [^{18}F]AlF-labeled antibody fragment preparation.

dx.doi.org/10.1021/bc4004926 | *Bioconjugate Chem.* 2014, 25, 335−341

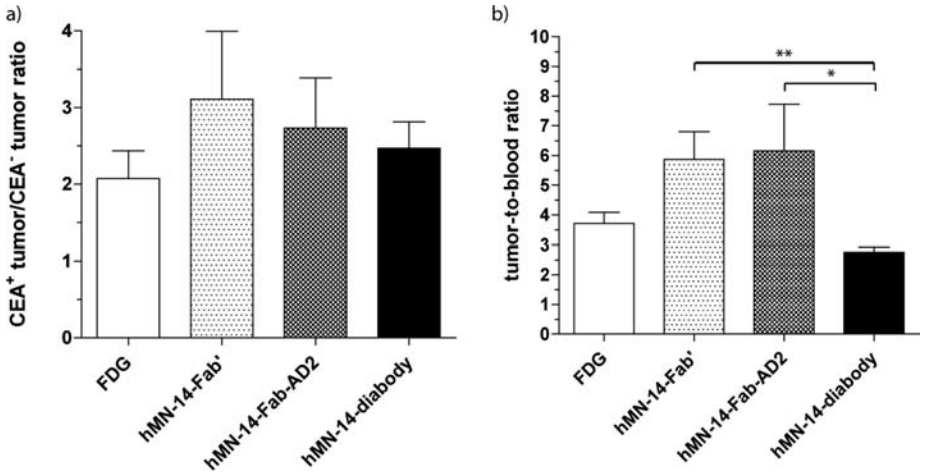

Figure 5. (a) CEA^+-to-CEA^- tumor, and (b) tumor-to-blood ratios of [^{18}F]-FDG, [^{18}F]AlF-hMN-14-Fab′, [^{18}F]AlF-hMN-14-Fab-AD2, and [^{18}F]AlF-hMN-14-diabody (*t* test: * $p = 0.0032$, ** $p = 0.0132$).

xenografts in order to show the applicability of [^{18}F]AlF-fluorination for heat-sensitive biomolecules and to characterize the optimal antibody formats to image CEA-expressing colorectal cancer.

The immunoreactivity of the [^{18}F]AlF-fluorinated antibody formats was preserved during the labeling procedure. The IC_{50} analyses indicated that the affinities of hMN-14-Fab′ and hMN-14-diabodies for CEA were comparable to that of hMN-14 IgG while the affinity of hMN-14-Fab-AD2 to CEA was slightly lower. Theoretically, the combination of [^{18}F]AlF and the diabody formats is particularly promising because the diabody fragment might benefit from bivalent binding. However, the results of the competitive binding assay indicate that bivalent binding does not provide significant advantages for the affinity.

In vivo, preferential localization of all [^{18}F]AlF-fluorinated antibody formats in the CEA^+ xenografts was observed, demonstrating feasibility of these [^{18}F]AlF-fluorinated antibody derivatives for imaging of CEA-expressing tumors. For hMN-14-Fab′ and [^{18}F]AlF-hMN-14-Fab-AD2, tumor-to-blood ratios were significantly higher compared to those of [^{18}F]AlF-hMN-14-diabody.

Liver uptake of both [^{18}F]AlF-hMN-14-Fab′ and [^{18}F]AlF-hMN-14-Fab-AD2 fragments was significantly lower compared to that of the diabody. Apparently, the diabody cleared partly via the hepatobiliary route. Consequently, visualization of liver metastases or tumors located in the liver can be obscured. Therefore, future studies will have to focus on decreasing the hepatic uptake of [^{18}F]AlF-fluorinated antibody formats.

In contrast, renal accumulation of the [^{18}F]AlF-hMN14-diabody derivative was significantly lower compared to that of the [^{18}F]AlF-hMN-14-Fab′ and [^{18}F]AlF-hMN-14-Fab-AD2 fragments. The high accumulation in the kidneys most likely is a consequence of tubular reabsorption after glomerular filtration of the [^{18}F]AlF-fluorinated antibody formats. This renal retention of [^{18}F]AlF-fluorinated antibody derivatives might hamper visualization of tumors located in the vicinity of the kidneys. The lower renal accumulation of the [^{18}F]AlF-hMN14-diabody derivative is most likely due to the bivalency of the derivative, leading to slower clearance from the blood, which results in lower renal accumulation at early time points after injection.

With the development of new molecular imaging agents, the number of applications for diagnostic PET imaging continues to increase. Several positron-emitting radionuclides are used for PET imaging, such as ^{64}Cu, ^{68}Ga, ^{124}I, ^{86}Y, and ^{89}Zr. Labeling of Fab′, F(ab′)$_2$, and scFv antibody fragments as well as mini- and diabodies with these radioisotopes has been described by several groups.[5−8] Smith-Jones et al. chelated ^{68}Ga to DOTA-conjugated F(ab′)$_2$ fragments of the anti-HER2 antibody Herceptin (trastuzumab) (^{68}Ga-DCHF) to demonstrate that ^{68}Ga-DCHF can be used to serially image HER2 expression in breast cancer xenografts.[9]

Eder et al.[7] evaluated the role of several recombinant anti-EpCAM scFv antibody fragments and diabodies for imaging of EpCAM-expressing tumors with ^{68}Ga. They demonstrated that PET imaging of solid tumors with a ^{68}Ga-labeled anti-EpCAM diabody format is feasible using *N*,*N*′-bis[2-hydroxy-5-(carboxyethyl)benzyl]ethylenediamine-*N*,*N*′-diacetic acid (HBED-CC) as a chelate.

Wu and colleagues[10] evaluated the tumor targeting capacity of the anti-CEA minibody based on the T84.66 antibody labeled with ^{64}Cu, using DOTA as a chelate, in mice with s.c. LS174T tumors, and they showed the feasibility of this format to image colorectal cancer with PET, although hepatic uptake was relatively high. However, the half-life of ^{64}Cu (12.7 h) might be too long for certain *in vivo* imaging studies. Sundaresan et al.[11] compared the tumor targeting capacity of the ^{124}I-labeled anti-CEA T84.66 minibody to that of the ^{124}I-labeled T84.66 diabody in the same model, and they demonstrated specific visualization of the CEA^+ xenografts with PET imaging with both ^{124}I-labeled formats.

The most widely used radionuclide for PET is ^{18}F. ^{18}F has ideal properties for PET due to its low positron energy of 635 keV, which reveals optimal spatial resolution of PET images.[12] In addition, the lack of other emissions and wide availability of the cyclotron-produced ^{18}F are advantageous for PET. Moreover, the half-life of 109.8 min permits more complex and time-consuming synthetic manipulations and biological studies. However, in general the labeling of biomolecules of ^{18}F is cumbersome. The labeling procedures for ^{68}Ga, in contrast, are relatively straightforward, because ^{68}Ga can be chelated with macrocyclic chelates such as DOTA or NOTA. In addition, ^{68}Ga is generated by a ^{68}Ge/^{68}Ga generator, allowing ^{68}Ga generation on-demand without the need for an on-site cyclotron. However, ^{68}Ge/^{68}Ga generators are not widely available and the relatively short half-life of 67.6 min restricts

dx.doi.org/10.1021/bc4004926 | *Bioconjugate Chem.* 2014, 25, 335−341

the use of ^{68}Ga. Additionally, ^{68}Ga has higher positron energy than ^{18}F, which limits the resolution of the PET images.

Despite these limitations, ^{68}Ga has been used in *in vivo* studies with antibodies and antibody fragments more frequently than ^{18}F, because of the more complex ^{18}F-labeling process, requiring labeling of a prosthetic group, deprotection, and subsequent conjugation to a protein.[13] The most widely used approaches for ^{18}F-labeling of biomolecules are based on the use of *N*-succinimidyl-4-[^{18}F]fluorobenzoate (SFB)[14] or [^{18}F]-fluorobenaldehyde.[15]

The [^{18}F]AlF labeling method developed by McBride et al.[2] provides a promising alternative to previous ^{18}F radiolabeling methods, as it can be efficiently performed in one step. However, this method requires a heating step to 100 °C to chelate [^{18}F]AlF. This step limited the procedure to heat-stable peptides and molecules that tolerate high temperatures. Recently, McBride et al. showed that the method can be used to label heat-sensitive biomolecules using a two-step method.[3] In this method, the NODA-MPAEM ligand is labeled with [^{18}F]AlF first, followed by conjugation to the biomolecule via its thiol group at room temperature. Here, we demonstrated the feasibility of this two-step method to label heat-sensitive biomolecules with ^{18}F *in vitro* and *in vivo*.

Taken together, all three [^{18}F]AlF-fluorinated antibody derivatives show high tumor-to-background ratios, allowing microPET imaging of CEA-expressing tumors. While the CEA$^+$/CEA$^-$ tumor ratios of all three antibody formats were comparable, significantly higher tumor-to-blood ratios were reached with the [^{18}F]AlF-hMN-14-Fab′ and [^{18}F]AlF-hMN-14-Fab-AD2 fragments, which resulted in slightly clearer visualization of CEA-expressing tumors with [^{18}F]AlF-hMN-14-Fab′ and [^{18}F]AlF-hMN-14-Fab-AD2. In addition, the lower hepatic uptake of [^{18}F]AlF-hMN-14-Fab′ and [^{18}F]AlF-hMN-14-Fab-AD2, compared to the [^{18}F]AlF-hMN-14-diabody format, might be advantageous for *in vivo* imaging of liver lesions. However, further research is needed to further decrease hepatic uptake of [^{18}F]AlF-fluorinated antibody fragments.

CONCLUSION

We demonstrated an efficient two-step method to label heat-sensitive biomolecules with ^{18}F and translated this method to preclinical PET imaging studies. *In vitro* and *in vivo* tumor targeting characteristics of [^{18}F]AlF-fluorinated hMN-14-Fab′, [^{18}F]AlF-hMN-14-Fab-AD2, and [^{18}F]AlF-hMN-14-diabody showed that all three antibody formats are promising candidates for PET imaging of CEA-expressing colorectal cancer.

AUTHOR INFORMATION

Corresponding Author

*MD Radboud University Medical Center, Dept. of Nuclear Medicine, P.O. Box 9101, 6500 HB Nijmegen, The Netherlands. Phone: +31-24-3615054. Fax: +31-24-3618942. E-mail: Susanne.Lutje@radboudumc.nl.

Notes

R.M.S., E.A.R., D.M.G., and W.J.M. are employed by and have stock in Immunomedics, Inc.

ACKNOWLEDGMENTS

We thank Bianca Lemmers-van de Weem, Henk Arnts, Iris Lamers-Elemans, and Kitty Lemmens-Hermans for their excellent technical assistance with the animal experiments.

ABBREVIATIONS

BSA, bovine serum albumin; CEA, carcinoembryonic antigen; DCHF, dichlorofluorescein; DIEA, *N*,*N*-diisopropylethylamine; DMF, dimethylformamide; DOTA, 1,4,7,10-tetraazacyclododecane-1,4,7,10-tetraacetic acid; EDTA, ethylenediaminetetraacetic acid; EM, *N*-(2-aminoethyl)maleimide; EpCAM, epithelial cell adhesion molecule; [^{18}F]FDG, 2-[^{18}F]fluoro-2-deoxyglucose; HBED-CC, *N*,*N*′-bis[2-hydroxy-5-(carboxyethyl)benzyl]ethylene diamine-*N*,*N*′-diacetic acid; HER2, human epidermal growth factor receptor 2; MPA, methyl phenylacetic acid; NHS, *N*-hydroxysuccinimide; NODA, 1,4,7-triazacyclononae-1,4-diacetate; NOTA, 1,4,7-triazacyclononane-1,4,7-triacetic acid; SD, standard deviation; [^{18}F]SFB, *N*-succinimidyl-4-[^{18}F]fluorobenzoate; SPECT, single photon emission computed tomography; TFA, trifluoroacetic acid; PBS, phosphate buffered serum; PET, positron emission tomography; % ID/g, percentage injected dose per gram

REFERENCES

(1) Volkow, N. D., Mullani, N. A., and Bendriem, B. (1988) Positron emission tomography instrumentation: an overview. *Am. J. Physiol. Imaging 3*, 142−153.

(2) McBride, W. J., Sharkey, R. M., Karacay, H., D'Souza, C. A., Rossi, E. A., Laverman, P., Chang, C.-H., Boerman, O. C., and Goldenberg, D. M. (2009) A novel method of ^{18}F radiolabeling for PET. *J. Nucl. Med. 50*, 991−998.

(3) McBride, W. J., D'Souza, C. A., Sharkey, R. M., and Goldenberg, D. M. (2012) The radiolabeling of proteins by the [^{18}F]AlF method. *Appl. Radiat. Isot. 70*, 200−204.

(4) Lindmo, T., Boven, E., Cuttitta, F., Fedorko, J., and Bunn, P. A., Jr. (1984) Determination of the immunoreactive fraction of radiolabeled monoclonal antibodies by linear extrapolation to binding at infinite antigen excess. *J. Immunol. Methods 72*, 77−89.

(5) Anderson, C. J., Connett, J. M., Schwarz, S. W., Rocque, P. A., Guo, L. W., Philpott, G. W., Zinn, K. R., Meares, C. F., and Welch, M. J. (1992) Copper-64-labeled antibodies for PET imaging. *J. Nucl. Med. 33*, 1685−1691.

(6) Cai, W., Chen, K., He, L., Cao, Q., Koong, A., and Chen, X. (2007) Quantitative PET of EGFR expression in xenograft-bearing mice using ^{64}Cu-labeled cetuximab, a chimeric anti-EGFR monoclonal antibody. *Eur. J. Nucl. Med. Mol. Imaging 34*, 850−858.

(7) Eder, M., Knackmuss, S., Le Gall, F., Reusch, U., Rybin, V., Little, M., Haberkorn, U., Mier, W., and Eisenhut, M. (2010) ^{68}Ga-labeled recombinant antibody variants for immuno-PET imaging of solid tumours. *Eur. J. Nucl. Med. Mol. Imaging 37*, 1397−1407.

(8) Robinson, M. K., Doss, M., Shaller, C., Narayanan, D., Marks, J. D., Adler, L. P., González Trotter, D. E., and Adams, G. P. (2005) Quantitative immuno-positron emission tomography imaging of HER2-positive tumor xenografts with an iodine-124 labeled anti-HER2 diabody. *Cancer Res. 65*, 1471−1478.

(9) Smith-Jones, P. M., Solit, D. B., Akhurst, T., Afroze, F., Rosen, N., and Larson, S. M. (2004) Imaging the pharmacodynamics of HER2 degradation in response to Hsp90 inhibitors. *Nat. Biotechnol. 22*, 701−706.

(10) Wu, A. M., Yazaki, P. J., Tsai, S. W., Nguyen, K., Anderson, A. L., McCarthy, D. W., Welch, M. J., Shively, J. E., Williams, L. E., Raubitschek, A. A., Wong, J. Y., Toyokuni, T., Phelps, M. E., and Gambhir, S. S. (2000) High-resolution microPET imaging of carcinoembryonic antigen-positive xenografts by using a copper-64-labeled engineered antibody fragment. *Proc. Natl. Acad. Sci. U. S. A. 97*, 8495−8500.

(11) Sundaresan, G., Yazaki, P. J., Shively, J. E., Finn, R. D., Larson, S. M., Raubitschek, A. A., Williams, L. E., Chatziioannou, A. F., Gambhir, S. S., and Wu, A. M. (2003) ^{124}I-labeled engineered anti-CEA minibodies and diabodies allow high-contrast, antigen-specific small-

animal PET imaging of xenografts in athymic mice. *J. Nucl. Med. 44*, 1962−1969.
(12) Visser, E. P., Disselhorst, J. A., Brom, M., Laverman, P., Gotthardt, M., Oyen, W. J., and Boerman, O. C. (2009) Spatial resolution and sensitivity of the Inveon small-animal PET scanner. *J. Nucl. Med. 50*, 139−147.
(13) Miller, P. W., Long, N. J., Vilar, R., and Gee, A. D. (2008) Synthesis of ^{11}C, ^{18}F, ^{15}O, and ^{13}N radiolabels for positron emission tomography. *Angew. Chem., Int. Ed. Engl. 47*, 8998−9033.
(14) Lang, L., and Eckelman, W. C. (1994) One-step synthesis of ^{18}F labeled [^{18}F]-N-succinimidyl 4-(fluoromethyl)benzoate for protein labeling. *Appl. Radiat. Isot. 45*, 1155−1163.
(15) Poethko, T., Schottelius, M., Thumshirn, G., Hersel, U., Herz, M., Henriksen, G., Kessler, H., Schwaiger, M., and Wester, H. J. (2004) Two-step methodology for high-yield routine radiohalogenation of peptides: [^{18}F]-labeled RGD and octreotide analogs. *J. Nucl. Med. 45*, 892−902.